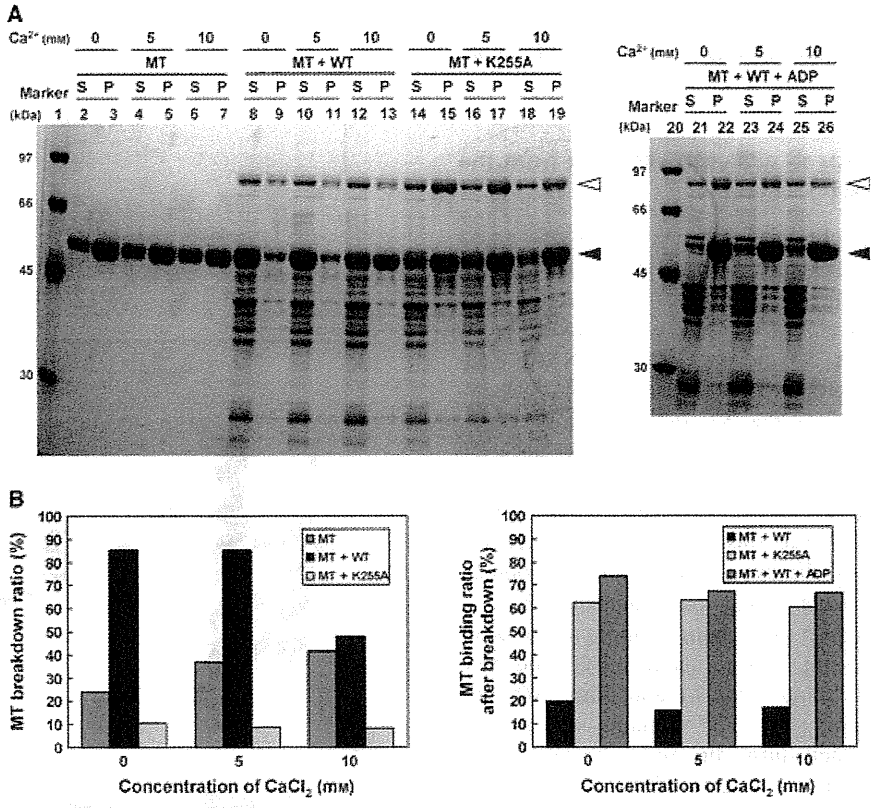

Fig. 5. The effects of Ca^{2+} on full-length p60-MT interactions. (A) *In vitro* MT cosedimentation assay performed with increasing Ca^{2+} concentrations (0–10 mM) using GST-tagged p60-katanin (wild-type and K255A mutant) in the presense of ATP (left) or using GST-tagged p60-katanin (wild-type) in the presense of ADP without Mg^{2+} (right). Taxol-stabilized MTs and associated p60-katanin were separated from depolymerized tubulin and unbound p60-katanin by sedimentation in a glycerol cushion buffer. P and S represent the pellet fraction and the supernatant fraction, respectively. Molecular sizes are shown in lane 1. Open and filled arrowheads indicate GST-tagged p60-katanin and tubulin, respectively. The SDS/PAGE gel was stained with Coomassie Brilliant blue. (B) Quantitative analysis of degraded tubulin fragments from taxol-stabilized MTs (left) and p60-katanin fragments binding to MT after degradation (right). Signals corresponding to the MT/tubulin and p60-katanin fragments in (A) were integrated and normalized by their molecular weights, using IMAGEJ.

between full-length p60-katanin and MTs in a cosedimentation assay. We quantified a normalized amount of the degraded tubulin fragments from taxol-stabilized MTs (Fig. 5B, left) and p60-katanin cosedimented with the remaining MT filaments (Fig. 5B, right). In the absence of p60-katanin, marked depolymerization of MT was observed in a Ca^{2+}-dependent manner, probably caused by a catastrophe effect [24] (Figs 5A, lanes 2–7 and 5B, left). In the presence of wild-type p60-katanin, most of the MTs were severed by p60-katanin (Figs 5A, lanes 8–11 and 5B, left). However, MT severing by p60-katanin was mostly inhibited by the presence of 10 mM Ca^{2+} (Figs 5A, lanes 12 and 13 and 5B, left). We observed a partial inhibition in the presence of 5 mM Ca^{2+} in multiple independent experiments (data not shown), thus we concluded that 5 mM of Ca^{2+} is an approximate threshold concentration for the inhibition of MT severing.

We further examined the MT-binding activity of p60-katanin using a K255A mutant that lacks ATPase activity (data not shown). K255A bound to MTs regardless of the Ca^{2+} concentration (Figs 5A, lanes 14–19 and 5B, right). Furthermore, K255A might stabilize MTs, because the Ca^{2+}-dependent catastrophe of MTs was suppressed (Figs 5A, left, lanes 14–19 and 5B, left). Recently, McNally & McNally [19] showed that ATPase-deficient katanin promoted the assembly of meiotic spindles. Our observation of K255A is partially consistent with their result. In addition, we examined the MT-binding activity of p60-katanin with ADP in the absence of Mg^{2+}. p60-katanin with ADP bound to MTs without MT severing regardless of the

Ca^{2+} concentration (Fig. 5A, right). Taken together, we concluded that Ca^{2+} inhibits the MT-severing activity of p60-katanin without affecting its MT-binding activity.

Ca^{2+} directly binds to p60-vMIT different from the interface with MT

With the aim of obtaining information on the possible involvement of metal ions in the action mechanism of p60-vMIT, we examined its interaction with Ca^{2+}, and with Ce^{3+} as an ideal paramagnetic probe for Ca^{2+} (Figs 6A, S3 and S4A) [25,26]. NMR titration analyses of p60-vMIT at various Ca^{2+} concentrations are shown in Fig. S3. In the case of Ca^{2+}, residues showing a major chemical shift perturbation were V66, I69 and K71. Because these residues are adjacent to the C-terminus of p60-katanin vMIT domain (residues 1–72), this binding site is assumed to be an artifact of the use of the engineered domain-only construct. When using paramagnetic Ce^{3+} to enhance the chemical shift changes upon metal binding, residues showing a large change, D23 and S24, were additionally found (Figs 6A and S4A). We succeeded in determining this Ce^{3+} binding site by analyzing pseudocontact shifts due to Ce^{3+} (Fig. S4B). The metal was chelated close to D23 and S24. From these results, we assumed that D23 and S24, which are evolutionarily conserved among many higher eukaryotes, form the binding site for Ca^{2+}. This Ca^{2+}-binding site differs from the putative interface between p60-vMIT and tubulin/MT, and so is consistent with our observation that Ca^{2+} did not inhibit MT binding.

From the structural model of the p60–MT complex, we hypothesized that the Ca^{2+}-binding site is close to the putative interface between the vMIT domain and hexameric AAA ATPase domains (Figs 6B,C and S5), enabling us to propose a model for the regulatory role of the vMIT domain in MT severing (Fig. 7). p60-katanin may form a putative ring-shaped hexamer, as indicated by Hartman & Vale [17]. We assumed that hexameric p60-katanin possesses flexible linkers between the vMIT and AAA domains, and may move over MTs using them freely. In the absence of Ca^{2+}, the ATPase activity of p60-katanin is elevated upon binding to an MT through contact between the vMIT and AAA domains. The enhanced activity of p60-katanin may lead to MT severing. After the reaction, p60-katanin is released from the MT and goes back to the basal state. In the presence of Ca^{2+}, however, p60-katanin does not adopt the activated state regardless of MT binding.

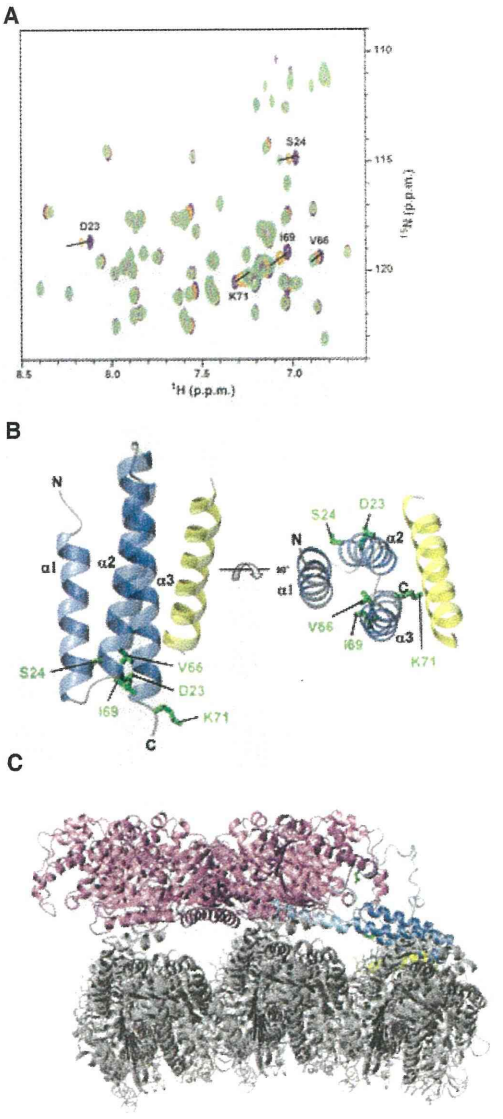

Fig. 6. Ca^{2+}-binding sites of p60-katanin. (A) ^1H–^{15}N HSQC spectra of p60-vMIT in the absence (violet) and presence of 1 mM (orange) and 2 mM (pale green) Ce^{3+} as a paramagnetic probe for Ca^{2+}. Residues with the greatest chemical shift perturbations are shown. (B) Side and top views of the ribbon diagram of p60-vMIT (PDB: 2rpa). Side chains of residues binding Ca^{2+} are shown in green. Tubulin helix 12, a putative interface of p60-vMIT, is colored yellow. (C) Proposed model for tubulin binding with full-length p60-katanin. Model complex between tubulin origomer (gray) and hexameric full-length p60-katanin, composed of p60-vMIT (blue), a coiled-coil (light blue), a flexible linker (light blue) and AAA ATPase (violet) domains is shown. One of the six p60-vMITs on the hexameric AAA ATPase is drawn. One helix 12 on tubulin, the putative interface of p60-katanin, is colored yellow. Residues bound to Ca^{2+} on p60-vMIT and residues on hexameric AAA ATPase domains close to the Ca^{2+}-binding sites on p60-vMIT are shown in green.

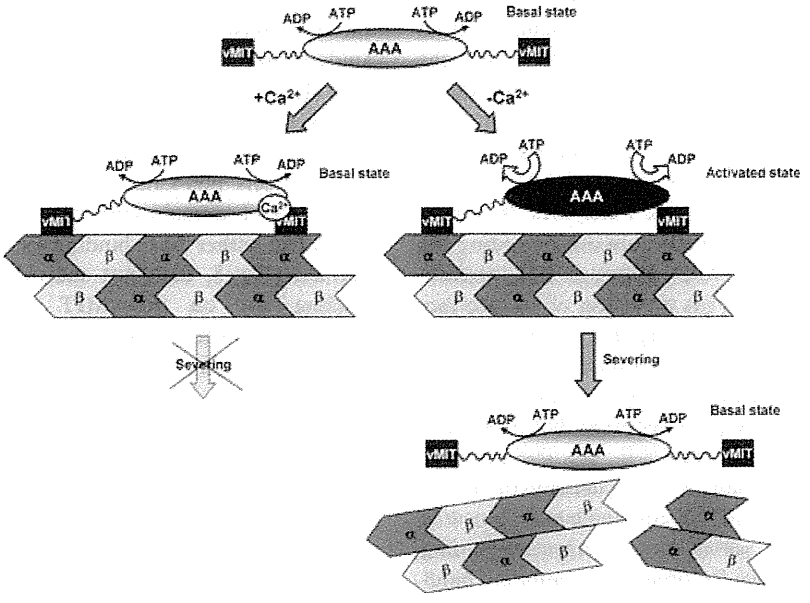

Fig. 7. Model of the mechanism of MT-severing by p60-katanin in the absence and presence of Ca^{2+}. Hexameric p60-katanin represents the enzyme in a basal state of ATP-dependent ATPase activity. Four of the six p60-vMIT domains, followed by flexible linkers on the side view of the hexameric AAA ring are not drawn for clarify. In the absence of Ca^{2+}, p60-katanin is in an activated state, whereby its ATPase activity is elevated by binding MT through an interaction between the vMIT and AAA domains, resulting in MT-severing. By contrast, when p60-katanin binds Ca^{2+}, p60-katanin remains in a basal state regardless of MT-binding and does not sever MT.

Discussion

The function of p80-CTD to capture and release p60-vMIT

Our NMR and mutation studies suggest that p80-CTD binds to a wide surface of p60-MIT, especially helix 1/2 and helix 1/3, which differs from the MT-binding surface, helix 2/3 (Figs 2B and S1B) [14]. If so, p80-CTD and MT could simultaneously bind to p60-vMIT, forming a ternary complex. However, our ATPase assay showed only a limited additive effect of p80-CTD and MT on ATPase activity (Fig. S2A). In addition, p80-CTD was excluded from the p60/MT complex (Fig. S6, lanes 9–12). Thus, in our experiments, we did not observe a ternary complex of p80-CTD, p60-vMIT and MT. Steric hindrance caused by p80-CTD binding to the surfaces of helices 1/2 and 1/3 may occur. This unique activity of p80-CTD may explain how adaptor-p80 recruits p60-katanin to MTs. That is, using the N-terminal WD40 domain, adaptor-p80 might localize on the γ-tubulin ring complex at the minus end of an MT [6], whereas p80-CTD captures p60-vMIT. p60-katanin would then relocate to the MT, whereas p80-CTD releases p60-vMIT. Note that, the *in vivo* activity of adaptor-p80 against p60-katanin also remains controversial, because adaptor-p80 localizes p60-katanin to the γ-tubulin ring complex and stimulates MT severing [8], whereas overexpression of adaptor-p80 suppress the MT-severing activity of p60-katanin in certain types of cell [11].

Existence of an MT-/p80-activated state of p60-katanin

The phenomenon that MT (substrate) as well as p80 (adaptor) binding to p60-katanin increases the ATPase activity of p60-katanin has been reported previously [6,17,18], although the molecular mechanism remains unclear. One explanation might be an equilibrium shift between an inactive dimeric state and an active hexameric state that forms upon binding to the substrate and/or adaptor. For example, the katanin-related type I AAA enzyme Vps4 has been shown to act in a dimer–hexamer equilibrium in a nucleotide-dependent manner, although substrate-dependent ATPase activation of Vps4 has not been reported to date [27,28]. Because multivalent binding between active katanin and MT is expected, MT-binding may promote hexamer formation in p60-katanin. We can rule out this possibility, however, because activation of ATP hydrolysis was observed even upon p60-katanin binding to p80-CTD, which was monomeric in solution (data not shown). This suggests the existence of a unique MT-/p80-activated state of p60-katanin. This activated

state of p60-katanin is more likely attributed to an allosteric effect depending on the intramolecular spatial rearrangement between the N-terminal vMIT and the central AAA domains, rather than an equilibrium shift.

The regulatory role of p60-vMIT on its own AAA domain has not been predicted. Nevertheless, it is not surprising if the analogy to other AAA-ATPases, including type II rather than type I enzymes, is considered. In general, the N-terminal domains preceding the AAA domain of type II AAA enzymes may perform three molecular functions: (a) provision of an interface for substrates for ATP hydrolyzing energy; (b) provision of an interface for adaptor proteins that mainly contribute to subcellular localization; and (c) modulation of ATPase activity. We previously reported that p60-vMIT serves as an interface for MTs [14]. We also reported that the N-terminal domain of both valosin-containing protein (VCP)/p97 and *N*-ethylmaleimide-sensitive fusion protein (NSF) serves as the substrate-binding site, as well as the surface for organelle membrane binding [29]. However, it has been reported that binding to substrates or membranes regulates the ATPase activity of these proteins [30,31]. In VCP/p97, the residues at the contact site between the N-domain and the first AAA domain (D1-domain) were identified in conjunction with Paget's disease of the bone and front temporal dementia (e.g. R155, A232, T262, and N387) [30,31]. A nucleotide-dependent conformational change in the N-domain relative to the D1-domain was observed by X-ray crystallography [30,31]. A mutation on A232 (A232E), one of the key residues, is associated with increased disease severity [32]. Biochemically, an A232E mutant exhibits elevated ATPase activity [33]. In NSF, a similar mechanism in which the contact site between the N-domain and D1 is associated with enhancement of ATPase activity has also been identified [34]. Note that, although both the sequences and the structures of the N-terminal domains of katanin and the VCP/NSF family are rather different, the AAA domains are highly conserved. Finally, we illustrate the MT-activated state of p60-katanin in Fig. 6C, assuming that the edge of p60-vMIT comes close enough to these interfacial residues on the AAA domain with a minimum structural change upon MT binding. In this model, residues E397 and G237 of p60-katanin are highlighted, and correspond to the interfacial residue N387 and the key residue A232 in VCP, respectively.

Ca^{2+} alters the spatial domain rearrangement of p60-katanin in its MT-/p80-activated state

In this study, we showed that Ca^{2+} inhibits the MT-severing activity of katanin, as well as reducing its MT-elevated ATPase activity to basal levels. Although the mechanism of this modulation seems complicated, studying the effect of Ca^{2+} on p60-katanin may provide clues to the working model of MT severing, which is driven by ATP hydrolyzing energy and catalyzed by katanin, as shown in Fig. 6C. First, we showed that Ca^{2+} affects p60-katanin activity by directly binding to the vMIT domain (Fig. 6). By contrast, Ca^{2+} does not affect either MT binding or p80 binding by the domain (Fig. 5, data not shown). Because the Ca^{2+}-binding site on p60-vMIT is different from its MT-binding site, these observations are consistent. Next, we found that Ca^{2+} does not affect the basal ATPase activity level of p60-katanin in the absence of MT and/or adaptor-p80 (Fig. 4A). By contrast, Ca^{2+} has an effect only on the MT- and/or p80-elevated ATPase activity, but not the basal activity (Figs 4B,C and S2B). Because a flexible linker ($\sim$ 114 amino acids) connects the N-terminal vMIT domain and the AAA domain, this Ca^{2+} effect is difficult to explain unless these two domains move spatially close to each other. As discussed above, we assume the existence of the MT-/p80-activated state of p60-katanin in such a domain rearrangement. It is likely that Ca^{2+} affects this MT-/p80-activated state, while the relative orientation of the two domains, which may be a trigger to elevate ATP hydrolysis, is altered by Ca^{2+}. This idea is further assessed by visualizing the spatial locations of the vMIT domain, Ca^{2+} ion, and the putative interfacial residues on the AAA domain (Figs 6C and S5).

Biological implications of the regulatory role of Ca^{2+} in MT-severing by katanin

In this study, Ca^{2+} negatively regulated the MT-severing function of katanin. In other words, Ca^{2+} contributed to the stabilization of MTs by protecting MTs from attack by katanin. The interaction of Ca^{2+} with MTs has been extensively studied because the inhibitory effect of Ca^{2+} on the *in vitro* assembly of MTs was reported by Weisenberg [23]. Ca^{2+} has been shown to destabilize polymerization of MTs directly or indirectly. Serrano *et al.* [35] determined the Ca^{2+}-binding sites on both α- and β-tubulin molecules, which are major components of MTs, and demonstrated that tubulin deprived of these sites could still polymerize in the presence of high concentrations of Ca^{2+}. Ca^{2+} is also known to affect dynamic instability in the assembly of MTs: it enhances the rate of catastrophic degradation of MT [24]. Lefèvre *et al.* [15] showed that the Ca^{2+}-binding sites of tubulin overlap with the binding sites for microtubule-associated proteins, and thus

Ca^{2+} competed with microtubule-associated proteins, resulting in the disassembly of MTs.

The indirect effect of Ca^{2+} on MT destabilization via one of the microtubule-associated proteins, tau, has received increased attention [36]. Calpain, a calcium-dependent nonlysosomal cysteine protease, plays critical roles in the pathway. Tau is highly relevant to regulating MT polymerization, or something of that nature. Hyperphosphorylation of tau, however, abolishes its ability to bind tubulin and promote MT assembly. When MTs release hyperphosphorylated tau, the protein aggregates into paired helical filaments, which are the neuropathological hallmarks of Alzheimer's disease. There are at least three protein kinases responsible for the hyperphosphorylation; cyclin-dependent-kinase 5, glycogen synthase kinase 3β and dual-specificity tyrosine-phosphorylation-regulated kinase 1A [37–39]. The activity of all the three kinases is regulated by calpain, as follows. In the presence of high concentrations of Ca^{2+}, glycogen synthase kinase 3β is truncated by calpain, generating two fragments of ~ 40 and 30 kDa. Glycogen synthase kinase 3β truncation augments its kinase activity [40]. Cyclin-dependent-kinase 5 is also activated by proteolytic cleavage of its specific activator p35 by calpain [41]. Recently, dual-specificity tyrosine-phosphorylation-regulated kinase 1A was shown to be proteolyzed and activated by calpain in Alzheimer disease brain [42]. In addition, calpain directly degrades tau, which also causes its loss of MT-stabilizing activity [43,44].

To date, Ca^{2+} has not been thought to stabilize MTs, but rather to promote their disassembly, as mentioned above. Our new findings on katanin, however, show that Ca^{2+} can slow the disassembly of MTs, suggesting that the assembly and disassembly of MT is managed by a more complicated system than expected. Excess Ca^{2+} is generally harmful to MTs, both directly and indirectly. To survive an accidental increase in Ca^{2+}, cells may have developed various fail-safe mechanisms, one of which might be the Ca^{2+} inhibition of katanin, which would function to avoid the rapid breakdown of MTs for the survival of neuronal cells upon a transient Ca^{2+} flux.

In conclusion, we have shown that p60-katanin, a type I AAA ATPase, possesses a novel mechanism for regulating its own ATPase activity, probably via a 3D domain rearrangement between the N-terminal vMIT domain and the AAA domain. Ca^{2+} binds p60-vMIT at the edge of this domain, close to the contact site between vMIT and AAA. This putative arrangement may well explain why Ca^{2+} inhibits MT severing without inhibiting either ATPase activity or MT-binding.

Experimental procedures

Production of p80-CTD

We generated a multiple sequence alignment of the C-terminal sequences of adaptor-p80 excluding the N-terminal WD40 repeats (residues 1–269) using CLUSTAL X [45], from which we decided to clone sequences 480–614, 480–630 and 480–655 of human and mouse p80. Expression vectors for the recombinant glutathione *S*-transferase (GST)-tagged form of the human and mouse p80 fragments were constructed using PRESAT vector methodology [46], as derived from the pGEX-4T3 vector (GE Healthcare, Buckinghamshire, UK). Finally, p80 (480–655), termed p80-CTD, was used for further analysis because this construct produced a more soluble protein than the others. Human p80-CTD, prepared by expression in *Escherichia coli* BL21 (*DE3*), followed by affinity purification on glutathione–Sepharose (GE Healthcare, Buckinghamshire, UK) and thrombin digestion, was used for ATPase assays. The expression vector for the recombinant MBP-tagged p80-CTD of mouse was also constructed by a standard protocol using PCR, and ligated into the *Eco*RI–*Hin*dII sites of pMAL-c2X (NEB). The fusion protein was prepared by expression in *E. coli* BL21 (*DE3*), followed by affinity purification on amylose-sepharose (New England Biolabs, Ipswich, MA, USA), and used for NMR experiments and binding experiments with p60-vMIT.

Production of p60-katanin

The expression vector for the recombinant GST-tagged full-length p60-katanin of mouse was constructed by a standard protocol using PCR, and ligated into the *Bam*HI–*Sal*I sites of pGEX-6P3 (GE Healthcare, Buckinghamshire, UK) [14]. An Ala-substituted mutant (K255A) was engineered with the QuikChange site-directed mutagenesis kit (Stratagene, Santa Clara, CA, USA). Two complementary oligonucleotides with mutated sequences for each mutant were used as primers (Table S2). The fusion proteins were produced in *E. coli* JM109. Expression was induced with 0.1 mM isopropyl thio-β-D-galactoside, and Luria–Bertani cultures were grown overnight at 20 °C. For cosedimentation assays, GST-tagged proteins were purified with glutathione–Sepharose and eluted in elution buffer (50 mM Tris/HCl, pH 7.4, 100 mM NaCl, 1 mM dithiothreitol, 50 mM reduced glutathione, and 5% glycerol). For ATPase assays, proteins were eluted in elution buffer (20 mM Tris/HCl, pH 7.5, 100 mM NaCl, 1 mM dithiothreitol, 1 mM EGTA, 2 mM $MgCl_2$, 0.25 mM ATP, 0.02% Triton X-100 and 5% glycerol) after PreScission Protease digestion on the column.

Production of the recombinant GST-tagged p60-vMIT domains of mouse, including wild-type and Ala-substituted mutants, was carried out as described previously (Table S2) [14]. The fusion proteins were expressed in *E. coli* BL21

(*DE3*), affinity-purified on glutathione–Sepharose and dialyzed. These fusion proteins were used for MBP-tagged p80-CTD binding assays. For NMR spectroscopy, a 1-L culture was incubated with [^{15}N]-ammonium chloride as the sole nitrogen source by following a standard fermentation protocol at 25 °C. Purification of ^{15}N-labeled p60-vMIT was achieved by glutathione–Sepharose affinity chromatography followed by thrombin digestion, benzamidine–Sepharose chromatography and gel filtration using a Superdex 75 column (GE Healthcare, Buckinghamshire, UK). The complex of ^{15}N-labeled p60-vMIT with p80-CTD was purified from a mixture of ^{15}N-labeled GST-tagged p60-vMIT and non-labeled MBP-tagged p80-CTD prepared following FactorXa and thrombin digestion, respectively.

Continuous ATPase assays of p60-katanin

ATPase activity was measured using an ATP regenerating system. The reaction mixture contained 50 mM Tris/HCl, pH 7.5, 50 mM KCl, 2 mM $MgCl_2$, 2 mM phosphoenolpyruvate, 1 mM ATP, 50 $\mu g \cdot mL^{-1}$ pyruvate kinase, 50 $\mu g \cdot mL^{-1}$ lactate dehydrogenase and 0.2 mM NADH. The reactions were performed in the presence of 0.4 μM p60-katanin, and ATPase activity was measured by monitoring the decrease in NADH absorption at 340 nm at room temperature using a UV–Vis spectrophotometer (UV mini-1240; Shimadzu, Tokyo, Japan). The shifts in absorption at 340 nm caused by the addition of taxol-stabilizing MTs and p80-CTD were measured. The absorbance data were representative of two or three independent experiments and were normalized relative to the level of the time-point zero. ATP hydrolysis activity was then calculated and represented in the unit of micromoles of ATP hydrolyzed per min per mg of p60-katanin ($units \cdot mg^{-1}$).

In vitro binding experiments

MBP-p80 bound to amylose resin was incubated with lysate of GST-tagged p60-vMIT domains in binding buffer (20 mM Tris/HCl, pH 7.4, 200 mM NaCl and 1 mM EGTA) for 2 h at 4 °C. The beads were washed four times in wash buffer (20 mM Tris/HCl, pH 7.4, 200 mM NaCl and 1 mM EGTA). The associated proteins were analyzed by SDS/PAGE.

Cosedimentation assays for MT-binding and MT-severing activity of p60-katanin

Taxol-stabilized MTs (1 μM) and GST-tagged p60-katanin (3.5 μM) were incubated for 30 min at 25 °C in binding buffer (80 mM Pipes, pH 7.0, 2 mM $MgCl_2$, 1 mM EGTA, 1 mM ATP and 20 μM taxol). Reaction mixtures (50 μL) were spun through a glycerol cushion buffer (50% v/v glycerol in binding buffer; 100 μL) for 30 min at 100 000 ***g***. Supernatants and pellets ware analyzed by SDS/PAGE. The band intensity of proteins was quantified with IMAGEJ (National Institutes of Health, Bethesda, MD, USA) (http://rsbweb.nih.gov/ij/).

NMR experiments

^{1}H–^{15}N HSQC spectra of ^{15}N-labeled p60-vMIT in the presence or the absence of p80-CTD were acquired at 25 °C on a Bruker AVANCE III 600 MHz spectrometer equipped with a cryogenic probe. These samples were dissolved in 20 mM sodium phosphate, pH 7.5, and 150 mM NaCl, and the protein concentrations were below 50 μM because of the low solubility of p80-CTD. ^{1}H-^{15}N HSQC spectra for Ce^{3+} titration experiments were recorded using 0.1 mM ^{15}N-labeled p60-vMIT at 25 °C on a Bruker AVANCE 500 MHz spectrometer equipped with a cryogenic probe. ^{1}H-^{15}N HSQC spectra for Ca^{2+} titration experiments were similarly performed (Fig. S3). The samples were dissolved in 20 mM Hepes, pH 7.5, and 25 mM NaCl. All data were processed using NMRPIPE [47] and SPARKY [48] software. The position of the coordinating Ce^{3+} ion was calculated by using the program FANTASIAN [49] coupled with an inhouse grid-search program with 144 pseudocontact shift value of NH signals. For calculation the coordinates of hVps4b-MIT (PDB: 1wr0) and p60-vMIT (PDB: 2rpa) were used. All of the figures were prepared by MOLMOL [50].

Molecular modeling

A hexameric ring model of the AAA domains of p60-katanin was generated on the basis of the hexameric ring structure of p97 D1 (PDB: 1s3s) using MODELLER (version 9v6) (http://salilab.org/modeller/), as described previously [14]. A molecular model of the complex of p60-vMIT with a tubulin oligomer (PDB: 3du7) was constructed on the basis of the complex between Vps4a-MIT and CHMP1a (PDB: 2jq9) [51] by replacing each component corresponding to p60-vMIT and helix 12 of α-tubulin, respectively [14]. Finally, the complex model of full-length p60-katanin and part of an MT was built by connecting these two models by a flexible linker corresponding to residues 91–204, and by placing the hexameric AAA domain close to the vMIT domain. The model was adjusted and visualized using MOLMOL [50].

References

1 McNally FJ & Vale RD (1993) Identification of katanin, an ATPase that severs and disassembles stable microtubules. *Cell* **75**, 419–429.

2 Hazan J, Fonknechten N, Mavel D, Paternotte C, Samson D, Artiguenave F, Davoine CS, Cruaud C, Durr A, Wincker P *et al.* (1999) Spastin, a new AAA protein, is altered in the most frequent form of autosomal dominant spastic paraplegia. *Nat Genet* **23**, 296–303.

3 Errico A, Ballabio A & Rugarli EI (2002) Spastin, the protein mutated in autosomal dominant hereditary spastic paraplegia, is involved in microtubule dynamics. *Hum Mol Genet* **11**, 153–163.
4 Cox GA, Mahaffey CL, Nystuen A, Letts VA & Frankel WN (2000) The mouse fidgetin gene defines a new role for AAA family proteins in mammalian development. *Nat Genet* **26**, 198–202.
5 Frickey T & Lupas AN (2004) Phylogenetic analysis of AAA proteins. *J Struct Biol* **146**, 2–10.
6 Hartman JJ, Mahr J, McNally K, Okawa K, Iwamatsu A, Thomas S, Cheesman S, Heuser J, Vale RD & McNally FJ (1998) Katanin, a microtubule-severing protein, is a novel AAA ATPase that targets to the centrosome using a WD40-containing subunit. *Cell* **93**, 277–287.
7 McNally KP, Bazirgan OA & McNally FJ (2000) Two domains of p80 katanin regulate microtubule severing and spindle pole targeting by p60 katanin. *J Cell Sci* **113**, 1623–1633.
8 Buster D, McNally K & McNally FJ (2002) Katanin inhibition prevents the redistribution of gamma-tubulin at mitosis. *J Cell Sci* **115**, 1083–1092.
9 McNally K, Audhya A, Oegema K & McNally FJ (2006) Katanin controls mitotic and meiotic spindle length. *J Cell Biol* **175**, 881–891.
10 Baas PW & Qiang L (2005) Neuronal microtubules: when the MAP is the roadblock. *Trends Cell Biol* **15**, 183–187.
11 Yu W, Solowska JM, Qiang L, Karabay A, Baird D & Baas PW (2005) Regulation of microtubule severing by katanin subunits during neuronal development. *J Neurosci* **25**, 5573–5583.
12 Qiang L, Yu W, Andreadis A, Luo M & Baas PW (2006) Tau protects microtubules in the axon from severing by katanin. *J Neurosci* **26**, 3120–3129.
13 Iwaya N, Goda N, Unzai S, Fujiwara K, Tanaka T, Tomii K, Tochio H, Shirakawa M & Hiroaki H (2007) Fine-tuning of protein domain boundary by minimizing potential coiled coil regions. *J Biomol NMR* **37**, 53–63.
14 Iwaya N, Kuwahara Y, Fujiwara Y, Goda N, Tenno T, Akiyama K, Mase S, Tochio H, Ikegami T, Shirakawa M *et al.* (2010) A common substrate recognition mode conserved between katanin p60 and VPS4 governs microtubule severing and membrane skeleton reorganization. *J Biol Chem* **285**, 16822–16829.
15 Lefevre J, Chernov KG, Joshi V, Delga S, Toma F, Pastre D, Curmi PA & Savarin P (2011) The C terminus of tubulin, a versatile partner for cationic molecules: binding of Tau, polyamines, and calcium. *J Biol Chem* **286**, 3065–3078.
16 Sudo H & Baas PW (2011) Strategies for diminishing katanin-based loss of microtubules in tauopathic neurodegenerative diseases. *Hum Mol Genet* **20**, 763–778.
17 Hartman JJ & Vale RD (1999) Microtubule disassembly by ATP-dependent oligomerization of the AAA enzyme katanin. *Science* **286**, 782–785.
18 Stoppin-Mellet V, Gaillard J & Vantard M (2002) Functional evidence for *in vitro* microtubule severing by the plant katanin homologue. *Biochem J* **365**, 337–342.
19 McNally KP & McNally FJ (2011) The spindle assembly function of *Caenorhabditis elegans* katanin does not require microtubule-severing activity. *Mol Biol Cell* **22**, 1550–1560.
20 Sudo H & Maru Y (2008) LAPSER1/LZTS2: a pluripotent tumor suppressor linked to the inhibition of katanin-mediated microtubule severing. *Hum Mol Genet* **17**, 2524–2540.
21 Mitchison T & Kirschner M (1984) Dynamic instability of microtubule growth. *Nature* **312**, 237–242.
22 Walker RA, O'Brien ET, Pryer NK, Soboeiro MF, Voter WA, Erickson HP & Salmon ED (1988) Dynamic instability of individual microtubules analyzed by video light microscopy: rate constants and transition frequencies. *J Cell Biol* **107**, 1437–1448.
23 Weisenberg RC (1972) Microtubule formation *in vitro* in solutions containing low calcium concentrations. *Science* **177**, 1104–1105.
24 O'Brien ET, Salmon ED & Erickson HP (1997) How calcium causes microtubule depolymerization. *Cell Motil Cytoskeleton* **36**, 125–135.
25 Bertini I, Lee YM, Luchinat C, Piccioli M & Poggi L (2001) Locating the metal ion in calcium-binding proteins by using cerium(III) as a probe. *ChemBioChem* **2**, 550–558.
26 Bertini I, Janik MB, Lee YM, Luchinat C & Rosato A (2001) Magnetic susceptibility tensor anisotropies for a lanthanide ion series in a fixed protein matrix. *J Am Chem Soc* **123**, 4181–4188.
27 Gonciarz MD, Whitby FG, Eckert DM, Kieffer C, Heroux A, Sundquist WI & Hill CP (2008) Biochemical and structural studies of yeast Vps4 oligomerization. *J Mol Biol* **384**, 878–895.
28 Inoue M, Kamikubo H, Kataoka M, Kato R, Yoshimori T, Wakatsuki S & Kawasaki M (2008) Nucleotide-dependent conformational changes and assembly of the AAA ATPase SKD1/VPS4B. *Traffic* **9**, 2180–2189.
29 Shiozawa K, Goda N, Shimizu T, Mizuguchi K, Kondo N, Shimozawa N, Shirakawa M & Hiroaki H (2006) The common phospholipid-binding activity of the N-terminal domains of PEX1 and VCP/p97. *FEBS J* **273**, 4959–4971.
30 DeLaBarre B & Brunger AT (2005) Nucleotide dependent motion and mechanism of action of p97/VCP. *J Mol Biol* **347**, 437–452.
31 Tang WK, Li D, Li CC, Esser L, Dai R, Guo L & Xia D (2010) A novel ATP-dependent conformation in p97 N-D1 fragment revealed by crystal structures of disease-related mutants. *EMBO J* **29**, 2217–2229.

32 Watts GD, Wymer J, Kovach MJ, Mehta SG, Mumm S, Darvish D, Pestronk A, Whyte MP & Kimonis VE (2004) Inclusion body myopathy associated with Paget disease of bone and frontotemporal dementia is caused by mutant valosin-containing protein. *Nat Genet* **36**, 377–381.
33 Halawani D, LeBlanc AC, Rouiller I, Michnick SW, Servant MJ & Latterich M (2009) Hereditary inclusion body myopathy-linked p97/VCP mutations in the NH2 domain and the D1 ring modulate p97/VCP ATPase activity and D2 ring conformation. *Mol Cell Biol* **29**, 4484–4494.
34 Matveeva EA, May AP, He P & Whiteheart SW (2002) Uncoupling the ATPase activity of the N-ethylmaleimide sensitive factor (NSF) from 20S complex disassembly. *Biochemistry* **41**, 530–536.
35 Serrano L, Valencia A, Caballero R & Avila J (1986) Localization of the high affinity calcium-binding site on tubulin molecule. *J Biol Chem* **261**, 7076–7081.
36 Buee L, Bussiere T, Buee-Scherrer V, Delacourte A & Hof PR (2000) Tau protein isoforms, phosphorylation and role in neurodegenerative disorders. *Brain Res Brain Res Rev* **33**, 95–130.
37 Liang Z, Liu F, Grundke-Iqbal I, Iqbal K & Gong CX (2007) Down-regulation of cAMP-dependent protein kinase by over-activated calpain in Alzheimer disease brain. *J Neurochem* **103**, 2462–2470.
38 Li T, Hawkes C, Qureshi HY, Kar S & Paudel HK (2006) Cyclin-dependent protein kinase 5 primes microtubule-associated protein tau site-specifically for glycogen synthase kinase 3beta. *Biochemistry* **45**, 3134–3145.
39 Ryoo SR, Jeong HK, Radnaabazar C, Yoo JJ, Cho HJ, Lee HW, Kim IS, Cheon YH, Ahn YS, Chung SH *et al.* (2007) DYRK1A-mediated hyperphosphorylation of Tau. A functional link between Down syndrome and Alzheimer disease. *J Biol Chem* **282**, 34850–34857.
40 Goni-Oliver P, Lucas JJ, Avila J & Hernandez F (2007) N-Terminal cleavage of GSK-3 by calpain: a new form of GSK-3 regulation. *J Biol Chem* **282**, 22406–22413.
41 Lee MS, Kwon YT, Li M, Peng J, Friedlander RM & Tsai LH (2000) Neurotoxicity induces cleavage of p35 to p25 by calpain. *Nature* **405**, 360–364.
42 Qian W, Liang H, Shi J, Jin N, Grundke-Iqbal I, Iqbal K, Gong CX & Liu F (2011) Regulation of the alternative splicing of tau exon 10 by SC35 and Dyrk1A. *Nucleic Acids Res* **39**, 6161–6171.
43 Johnson GV, Jope RS & Binder LI (1989) Proteolysis of tau by calpain. *Biochem Biophys Res Commun* **163**, 1505–1511.
44 Yang LS & Ksiezak-Reding H (1995) Calpain-induced proteolysis of normal human tau and tau associated with paired helical filaments. *Eur J Biochem* **233**, 9–17.
45 Thompson JD, Gibson TJ, Plewniak F, Jeanmougin F & Higgins DG (1997) The CLUSTAL_X windows interface: flexible strategies for multiple sequence alignment aided by quality analysis tools. *Nucleic Acids Res* **25**, 4876–4882.
46 Goda N, Tenno T, Takasu H, Hiroaki H & Shirakawa M (2004) The PRESAT-vector: asymmetric T-vector for high-throughput screening of soluble protein domains for structural proteomics. *Protein Sci* **13**, 652–658.
47 Delaglio F, Grzesiek S, Vuister GW, Zhu G, Pfeifer J & Bax A (1995) NMRPipe: a multidimensional spectral processing system based on UNIX pipes. *J Biomol NMR* **6**, 277–293.
48 Goddard TD & Kneller DG (2004) *Sparky 3*. University of California, San Francisco.
49 Bertini I, Cremonini MA, Gori-Savellini G, Luchinat C, Wuthrich K & Guntert P (1998) PSEUDYANA fo NMR structure calculation of paramagnetic metalloproteins using torsion angle molecular dynamics. *J Biomol NMR* **12**, 553–557.
50 Koradi R, Billeter M & Wuthrich K (1996) MOLMOL: a program for display and analysis of macromolecular structures. *J Mol Graph* **14**, 29–32.
51 Stuchell-Brereton MD, Skalicky JJ, Kieffer C, Karren MA, Ghaffarian S & Sundquist WI (2007) ESCRT-III recognition by VPS4 ATPases. *Nature* **449**, 740–744.

Supporting information

The following supplementary material is available:
Fig. S1. Analyses of the interaction between p60-vMIT and p80-CTD.
Fig. S2. ATPase activity of full-length p60-katanin in the presence of MT, p80-CTD, and increasing concentrations of Ca^{2+}.
Fig. S3. ^{1}H-^{15}N HSQC spectra of p60-vMIT in the absence (black) and presence of 5 mM (magenta), 10 mM (cyan), 15 mM (yellow), 25 mM (green) Ca^{2+}.
Fig. S4. Ce^{3+} titration experiments of p60-vMIT.
Fig. S5. Close-up view of the Ca^{2+} binding region of p60-katanin in Fig. 6C.
Fig. S6. MT co-sedimentation assay in the presence of p60-katanin and p80-CTD *in vitro*.
Table S1. The broadened signals of ^{15}N-labeled p60-vMIT in the presence of p80-CTD.
Table S2. Oligonucleotides used as primers for Ala substitution.

This supplementary material can be found in the online version of this article.

Please note: As a service to our authors and readers, this journal provides supporting information supplied by the authors. Such materials are peer-reviewed and may be re-organized for online delivery, but are not copy-edited or typeset. Technical support issues arising from supporting information (other than missing files) should be addressed to the authors.

11282528_File000004_208922474.doc12/22/2011

Effect of Ca^{2+} on the microtubule-severing enzyme p60-katanin: insight into the substrate-dependent activation mechanism.

Naoko Iwaya[a,b], Kohei Akiyama[b,c], Natsuko Goda[b,c,d], Takeshi Tenno[a,b,d], Yoshie Fujiwara[b,e,f], Daizo Hamada[b,e], Teikichi Ikura[g], Masahiro Shirakawa[a] and Hidekazu Hiroaki[b,c,d,e]*

[a]Department of Molecular Engineering, Graduate School of Engineering, Kyoto University, Katsura, Nishikyo-ku, Kyoto 615-8530, Japan

[b]Division of Structural Biology, Graduate School of Medicine, Kobe University, 7-5-1 Kusunokicho, Chuo-ku, Kobe, Hyogo 650-0017, Japan

[c]Field of Supramolecular Biology, International Graduate School of Arts and Sciences, Yokohama City University

[d]Structural Biology Research Center and Division of Biological Science, Graduate School of Science, Nagoya University, Furo-cho, Chikusa-ku, Nagoya, Aichi 464-8601, Japan

[e]Global Center of Excellence Program for Integrative Membrane Biology, Kobe University

[f]Laboratory of Supramolecular Crystallography, Research Center for Structural and Functional Proteomics, Institute for Protein Research, Osaka University

[g]Graduate School of Biomedical Science, Tokyo Medical and Dental University

11282528_File000004_208922474.doc12/22/2011

Supplementary Table 1.
The broadened signals of ^{15}N-labeled p60-vMIT in the presence of p80-CTD.

loop 1	helix 1	loop 1-2	helix 2	loop 2-3	helix 3
S2	M5	G20	D23	S42	T46
L3	V7		S24	K44	H47
	E8		Y28		L48
	N9		G31		R49
	V10		V32		Q53
	K11		L33		E58
	L12		M36		Q65
	A13		Y39		V66
	R14		Y41		K67
	E15				D68
	Y16				
	L18				
	L19				

Supplementary Table 2.
Oligonucleotides used as primers for Ala substitution.

Primer	Sequence
K255A_F	CACCTGGCACTGGA**GCG**ACCCTTCTAGCTAAAG
K255A_R	CTTTAGCTAGAAGGGT**CGC**TCCAGTGCCAGGTG
K11A_F	CAAATGATTGTTGAGAATGTA**GCC**TTGGCTCGTGAATATGCACTG
K11A_R	CAGTGCATATTCACGAGCCAA**GGC**TACATTCTCAACAATCATTTG
E15A_F	GAGAATGTAAAATTGGCTCGT**GCC**TATGCACTGCTGGGAAACTATGAC
E15A_R	GTCATAGTTTCCCAGCAGTGCATA**GGC**ACGAGCCAATTTTACATTCTC
Y16A_F	GAGAATGTAAAATTGGCTCGTGAA**GCC**GCACTGCTGGGAAACTATGAC
Y16A_R	GTCATAGTTTCCCAGCAGTGC**GGC**TTCACGAGCCAATTTTACATTCTC
D23A_F	GCACTGCTGGGAAACTAT**GCC**TCTGCAATGGTCTACTATCAG
D23A_R	CTGATAGTAGACCATTGCAGA**GGC**ATAGTTTCCCAGCAGTGC
V27A_F	GGAAACTATGACTCTGCAATG**GCC**TACTATCAGGGAGTTCTTGAC
V27A_R	GTCAAGAACTCCCTGATAGTA**GGC**CATTGCAGAGTCATAGTTTCC
Y28A_F	GGAAACTATGACTCTGCAATGGTC**GCC**TATCAGGGAGTTCTTGAC
Y28A_R	GTCAAGAACTCCCTGATA**GGC**GACCATTGCAGAGTCATAGTTTCC
Q35A_F	CAGGGAGTTCTTGAC**GCC**ATGAACAAGTACCTGTACTCAGTC
Q35A_R	GACTGAGTACAGGTACTTGTTCAT**GGC**GTCAAGAACTCCCTG
N37A_F	CAGGGAGTTCTTGACCAAATG**GCC**AAGTACCTGTACTCAGTC
N37A_R	GACTGAGTACAGGTACTT**GGC**CATTTGGTCAAGAACTCCCTG
D45A_F	CTGTACTCAGTCAAA**GCC**ACACACCTCCGTCAGAAATGG
D45A_R	CCATTTCTGACGGAGGTGTGT**GGC**TTTGACTGAGTACAG
R49A_F	GTCAAAGATACACACCTC**GCC**CAGAAATGGCAACAG
R49A_R	CTGTTGCCATTTCTG**GGC**GAGGTGTGTATCTTTGAC
Q53A_F	CTCCGTCAGAAATGG**GCC**CAGGTTTGGCAGGAAATAAATGTG
Q53A_R	CACATTTATTTCCTGCCAAACCTG**GGC**CCATTTCTGACGGAG
Q54A_F	CTCCGTCAGAAATGGCAA**GCC**GTTTGGCAGGAAATAAATGTG
Q54A_R	CACATTTATTTCCTGCCAAAC**GGC**TTGCCATTTCTGACGGAG
V55A_F	CTCCGTCAGAAATGGCAACAG**GCC**TGGCAGGAAATAAATGTG
V55A_R	CACATTTATTTCCTGCCA**GGC**CTGTTGCCATTTCTGACGGAG
E58A_F	CAGAAATGGCAACAGGTTTGGCAG**GCC**ATAAATGTGGAAGCTAAG
E58A_R	CTTAGCTTCCACATTTAT**GGC**CTGCCAAACCTGTTGCCATTTCTG

11282528_File000004_208922474.doc12/22/2011

Primer	Sequence
K64A_F	GTTTGGCAGGAAATAAATGTGGAAGCT**GCC**CAAGTTAAGGATATCATG
K64A_R	CATGATATCCTTAACTTG**GGC**AGCTTCCACATTTATTTCCTGCCAAAC
K67A_F	GTGGAAGCTAAGCAAGTT**GCC**GATATCATGAAAACATAATAGAGC
K67A_R	GCTCTATTATGTTTTCATGATATC**GGC**AACTTGCTTAGCTTCCAC
D68A_F	GTGGAAGCTAAGCAAGTTAAG**GCC**ATCATGAAAACATAATAGAGC
D68A_R	GCTCTATTATGTTTTCATGAT**GGC**CTTAACTTGCTTAGCTTCCAC

11282528_File000004_208922474.doc12/22/2011

Supplementary Fig. 1.

Analyses of the interaction between p60-vMIT and p80-CTD. (A) ^{1}H-^{15}N HSQC spectra of p60-vMIT in the absence (black) and presence (red) of p80-CTD. Residues whose NH signals of p60-vMIT were broadening in the presence of p80-CTD are shown in red. Since a ^{1}H-^{15}N HSQC spectrum of p60-vMIT in the presence of p80-CTD was drastically broadening, it was represented at a high threshold level corresponding to the noise. (B) Residues whose NH signals of p60-vMIT were broadening in the presence of p80-CTD are mapped on the surface in red. Tubulin binding site of p60-vMIT is shown in yellow. The residues where the broadened signals and tubulin binding site overlap are shown in green. The surface orientations are shown by the ribbon diagram of p60-vMIT (PDB: 2rpa).

Supplementary Fig. 2.

ATPase activity of full-length p60-katanin in the presence of MT, p80-CTD, and increasing concentrations of Ca^{2+}. (A) ATPase activity of p60-katanin (0.4 μM) was monitored at 340 nm in the absence (black diamond) and presence of 1 μM taxol-stabilized MTs (gray diamond), 0.4 μM p80-CTD (open diamond), or both (asterisk). (B) The ATPase activity of p60-katanin (0.4 μM) + taxol-stabilized MTs (1 μM) + p80-CTD (0.4 μM) was monitored at 340 nm in the presence of increasing Ca^{2+} concentrations: 1 mM (gray triangle), 2 mM (black circle), and 5 mM (open square) (left). ATPase activity in presence of MTs and p80-CTD was further expressed as μmoles of ATP hydrolyzed per min per mg of p60-katanin (units/mg) in 0, 1, 2, and 5 mM of Ca^{2+} (right).

Supplementary Fig. 3.

^{1}H-^{15}N HSQC spectra of p60-vMIT in the absence (black) and presence of 5 mM (magenta),

10 mM (cyan), 15 mM (yellow), 25 mM (green) Ca^{2+}. Residues with the greatest chemical shift perturbations are shown.

Supplementary Fig. 4.

Ce^{3+} titration experiments of p60-vMIT. (A) ^{1}H-^{15}N HSQC spectra of p60-vMIT in the absence (violet) and presence of 1 mM (orange), 2 mM (pale green), 5 mM (red), 10 mM (blue) Ce^{3+} as a paramagnetic probe for Ca^{2+}. Residues with the greatest chemical shift perturbations are shown. (B) A view of best 5 positions of Ce^{3+} ion (orange) in p60-vMIT (PDB: 2rpa). Side chains of residues binding Ce^{3+} are shown in green. The position of the coordinating Ce^{3+} ion was calculated by using the program FANTASIAN (http://www.cerm.unifi.it./softwares/software- fantasian) coupled with an inhouse grid-search program with 144 pseudocontact shift value of NH signals.

Supplementary Fig. 5.

Close-up view of the Ca^{2+} binding region of p60-katanin in Fig. 6C.

Supplementary Fig. 6.

MT co-sedimentation assay in the presence of p60-katanin and p80-CTD *in vitro*. The assay used a GST-tagged K255A mutant p60 and MBP-tagged p80-CTD. MTs and associated proteins were separated from unbound proteins by sedimentation in a glycerol cushion buffer. The proteins used for co-sedimentation are indicated at the top of the gel. P and S represent the pellet fraction and the supernatant fraction, respectively. Molecular sizes are shown in lanes 1 and 8. Open, gray and filled arrowheads show GST-tagged p60, MBP-tagged p80-CTD and MT, respectively. The SDS-PAGE gel was stained with Coomassie blue.

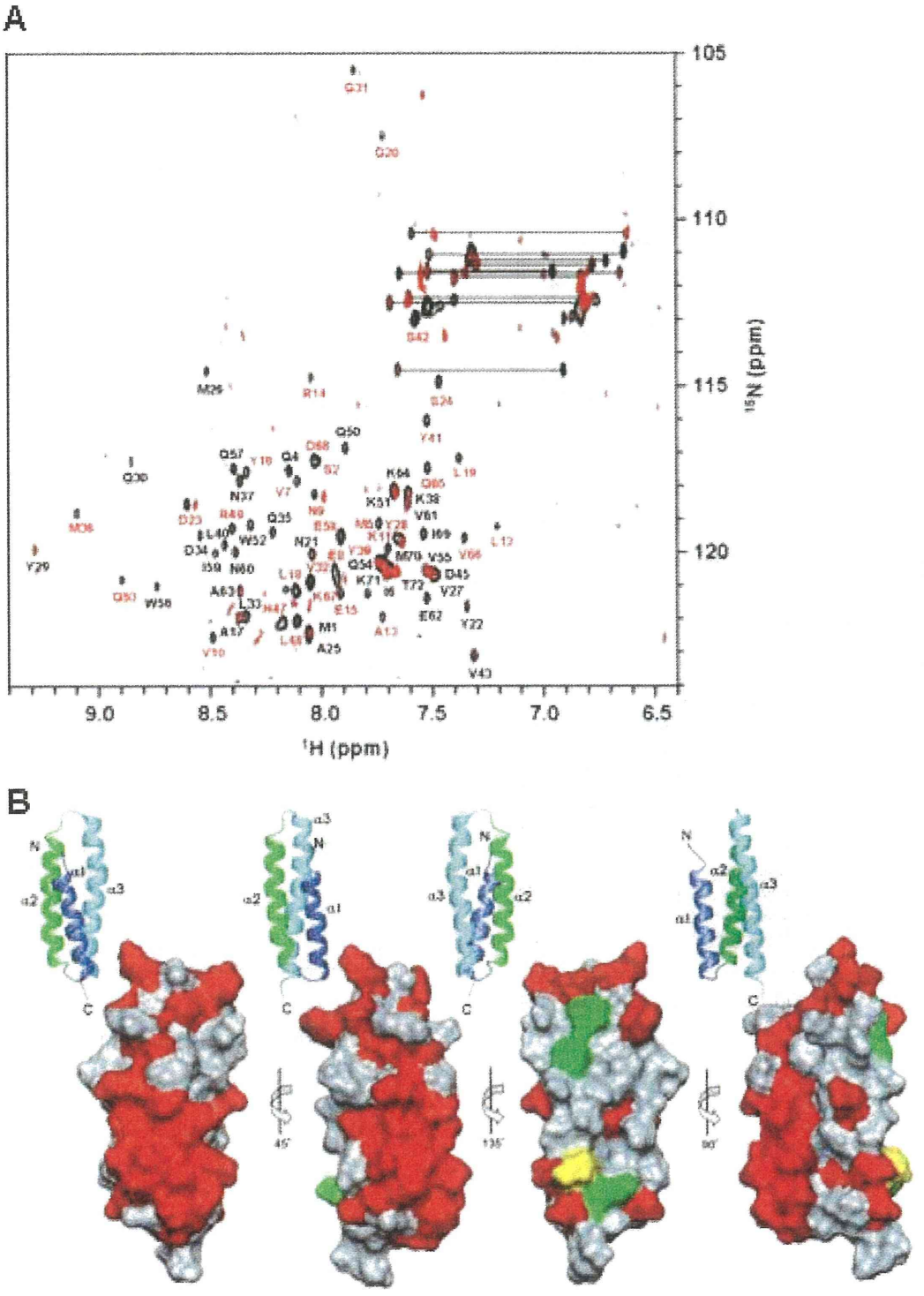

Supplementary Figure 1

11282528_File000004_208922474.doc12/22/2011

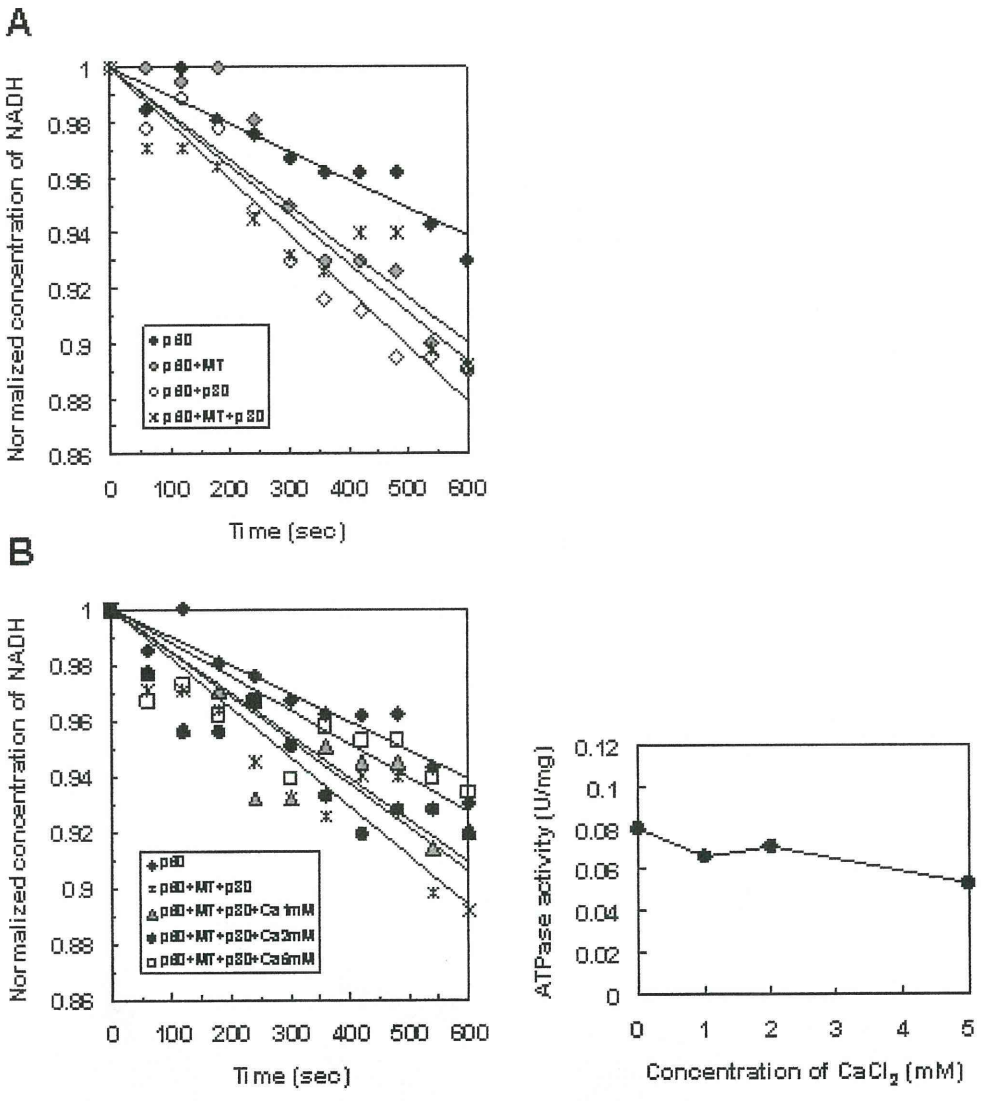

Supplementary Figure 2

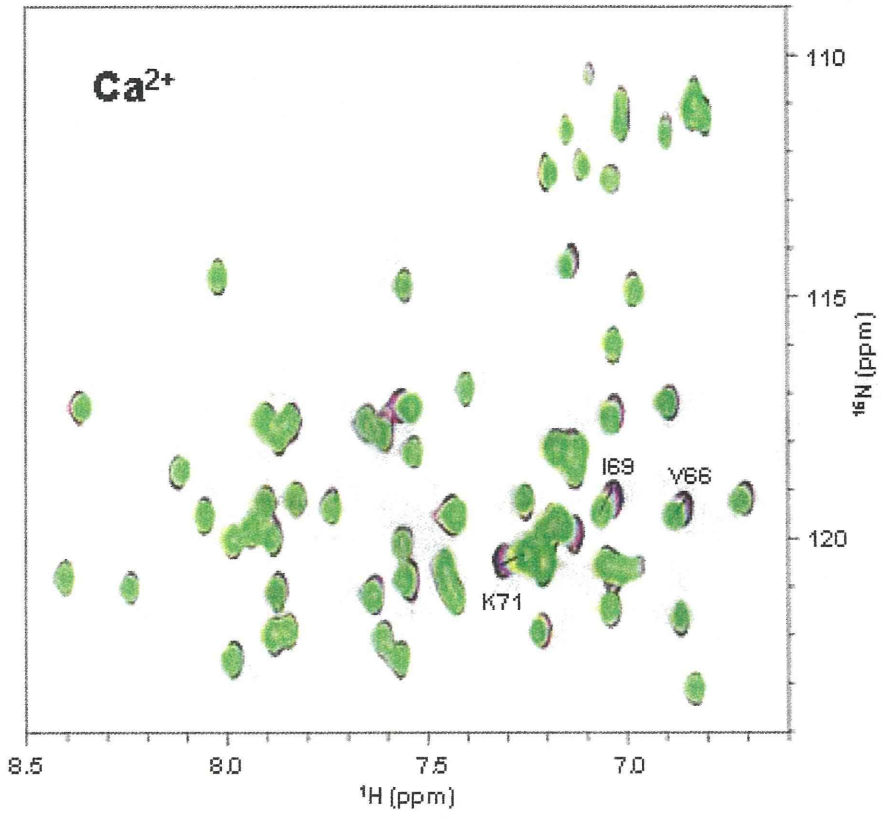

Supplementary Figure 3

11282528_File000004_208922474.doc12/22/2011

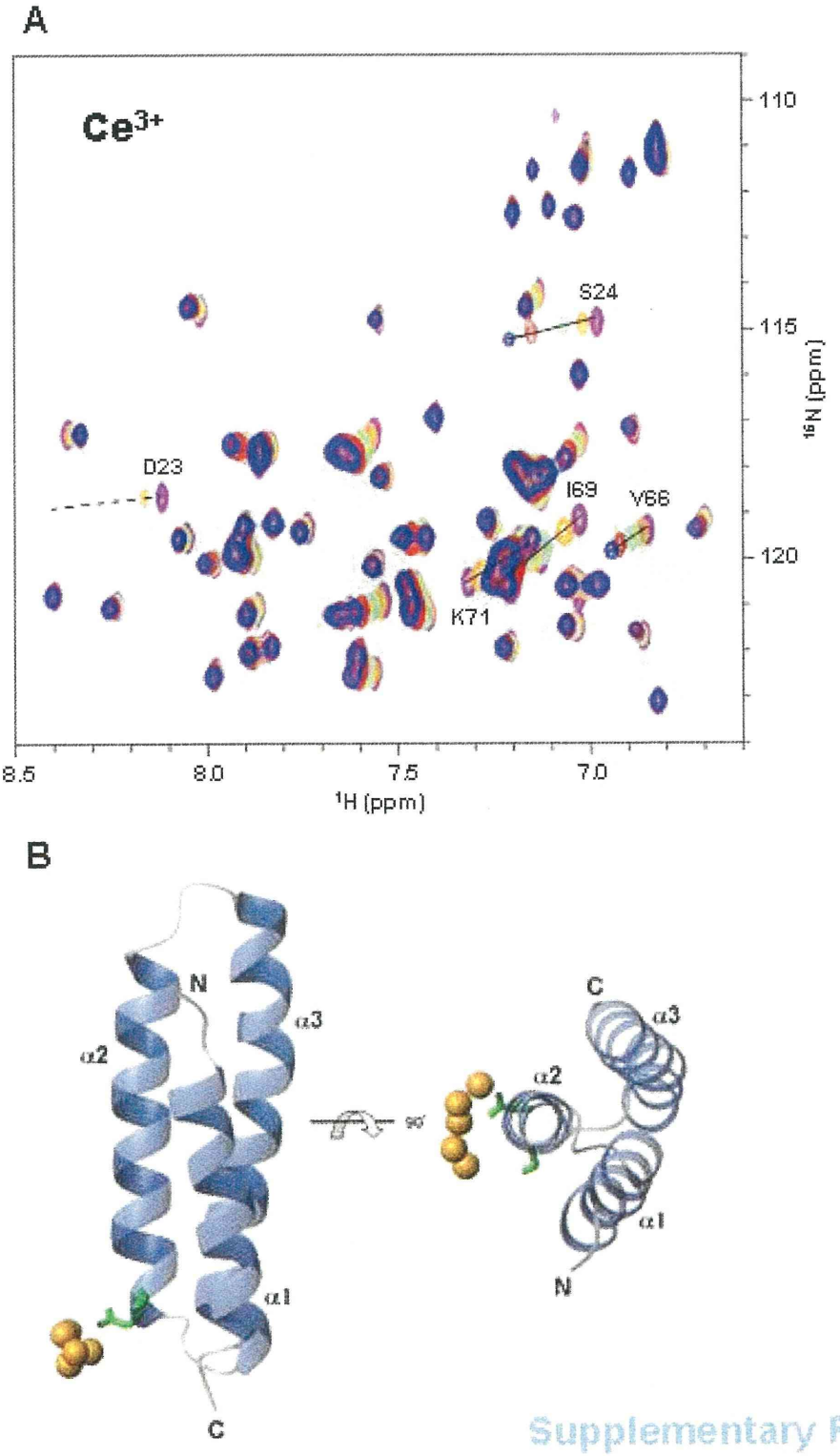

Supplementary Figure 4

11282528_File000004_208922474.doc12/22/2011

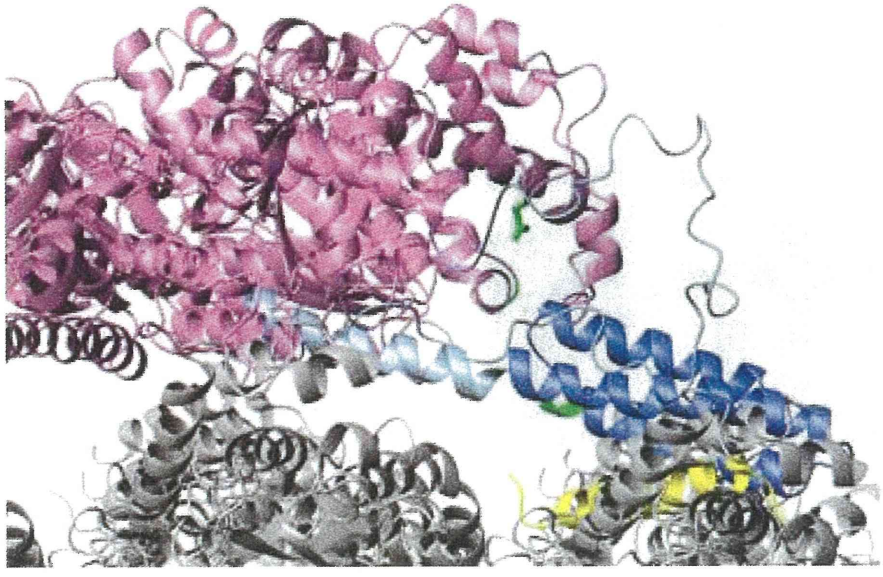

Supplementary Figure 5

11282528_File000004_208922474.doc12/22/2011

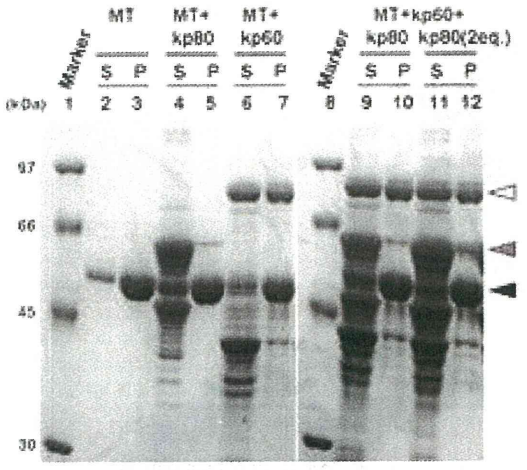

Supplementary Figure 6